

Coherent scattering of near-resonant light by a Dense Microscopic Cold Atomic cloud

S. Jennewein,¹ M. Besbes,¹ N.J. Schilder,¹ S.D. Jenkins,² C. Sauvan,¹
J. Ruostekoski,² J.-J. Greffet,¹ Y.R.P. Sortais,¹ and A. Browaeys¹

¹*Laboratoire Charles Fabry, Institut d'Optique, CNRS, Univ Paris Sud,
2 Avenue Augustin Fresnel, 91127 Palaiseau cedex, France*

²*Mathematical Sciences, University of Southampton, Southampton SO17 1BJ, United Kingdom*
(Dated: April 29, 2016)

We measure the coherent scattering of light by a cloud of laser-cooled atoms with a size comparable to the wavelength of light. By interfering a laser beam tuned near an atomic resonance with the field scattered by the atoms we observe a resonance with a red-shift, a broadening, and a saturation of the extinction for increasing atom numbers. We attribute these features to enhanced light-induced dipole-dipole interactions in a cold, dense atomic ensemble that result in a failure of standard predictions such as the “cooperative Lamb shift”. The description of the atomic cloud by a mean-field model based on the Lorentz-Lorenz formula that ignores scattering events where light is scattered recurrently by the same atom and by a microscopic discrete dipole model that incorporates these effects lead to progressively closer agreement with the observations, despite remaining differences.

The understanding of light propagation in dense media relies traditionally on a continuous description of the sample characterized by macroscopic quantities such as susceptibility or refractive index [1, 2]. Their derivation from a microscopic theory is in general challenging owing to the interactions between the light-induced dipoles that can be large when the light is tuned near an atomic resonance. In dilute media, their role can be analyzed using the perturbative approach of Friedberg, Hartmann and Manassah (FHM) [3], which predicts in particular a “cooperative Lamb-shift” measured recently in inhomogeneously broadened media [4, 5] and cold dilute atomic gases [6]. For an atom slab, the FHM approach was shown to correspond to the low-density limit of the local-field model introduced by Lorentz [7], which replaces the action of all the atoms of the medium on a particular one by an average effective field [1, 2], thus ignoring correlations between the light-induced dipoles. This mean-field approach leads to the Lorentz-Lorenz formula, which allows calculating the index of refraction of many dense media with an excellent accuracy [1, 8]. However it was pointed out [7, 9] that in the absence of inhomogeneous broadening, such as in cold atomic ensembles, the mean-field response may not be valid due to recurrent scattering where the field radiated by one atom can be scattered back by another atom [10, 11]. Recurrent scattering should become important when the incident light (wavelength $\lambda = 2\pi/k$) is tuned near an atomic resonance, and the atomic density approaches k^3 . This calls for an experiment operating in this regime, where a comparison between the standard mean-field theories of light scattering and a microscopic approach including recurrent scattering can be performed.

Here, we perform this comparison. To do so we need to access a quantity relevant to both the macroscopic and the microscopic approaches. The *coherent* electric field $\langle \mathbf{E}_{\text{sc}} \rangle$ scattered by the cloud fulfills this condition: it is obtained by averaging the scattered field \mathbf{E}_{sc} over

many realizations of the spatial random distribution of atoms, and its evolution is governed by the macroscopic Maxwell’s equations in the cloud considered as an homogeneous medium described by a susceptibility. In the case of cold atomic gases, the near-resonance coherent optical response has been explored experimentally using mostly dilute, optically thick ensembles [12–19]. Recently, we studied the light scattered by a microscopic *dense* cloud of cold atoms at 90° of a near-resonant excitation laser [20]. In that situation, we were sensitive to the *incoherent* component $\langle |\mathbf{E}_{\text{sc}} - \langle \mathbf{E}_{\text{sc}} \rangle|^2 \rangle$ of the scattered light. We could therefore not compare our results with mean-field predictions for continuous media, which are only relevant for the coherent part.

In this work, we study the *coherent* scattering by our microscopic cloud. The cloud contains up to a few hundreds laser-cooled rubidium 87 atoms and has a size smaller than the wavelength of the optical D2 transition. We illuminate the sample with a tightly focused laser with a waist larger than the cloud size. We access the coherent scattering by measuring the extinction resulting from the interference of the laser field with the field scattered by the cloud. We observe a saturation of the extinction, a broadening of the line, and a small red-shift when we vary the number of atoms from 10 to 180. We show that the measured shift and width do not agree with the FHM perturbative approach. The description of the atomic cloud by a mean-field model based on the Lorentz-Lorenz formula also disagrees with our data. Finally a microscopic discrete dipole model that incorporates recurrent scattering leads to a qualitatively closer agreement with our measurements, despite remaining differences.

To study the coherent scattering by our cloud, we detect the interference in the far field between the laser field \mathbf{E}_{L} and the scattered field \mathbf{E}_{sc} . To do so, we use two identical aspherical lenses L1 and L2 with a high numerical aperture (NA=0.5) mounted in a confocal configuration

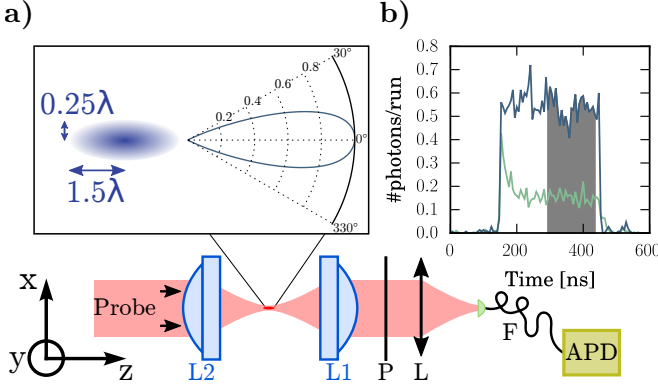


FIG. 1: (a) Experimental setup. A microscopic cloud of ^{87}Rb atoms is illuminated by a linearly-polarized probe laser focused down to a waist $w = 1.2 \mu\text{m}$. (P): polarizer. (L) Lens allowing the mode-matching between the laser probe beam and the single-mode fiber (F) in the absence of atoms. (APD): avalanche photo-diode. Inset: cloud rms widths (left) and intensity radiation pattern (right), calculated using a microscopic approach (see text). The coherent part, $|\mathcal{E}_{\text{coh}}(\omega)|^2$, dominates the incoherent part, which is more isotropic and is orders of magnitude smaller. (b) Example of temporal signals recorded on the APD with $N = 180$ atoms (green line) and without atoms (blue line). The laser is nearly resonant with the atoms, with a frequency detuning $\Delta = 0.3\Gamma$. Each run consists of 1000 illuminations with a duration of 300 ns each. Temporal bins: 6 ns. Grey area: time interval used for the steady-state analysis.

in a vacuum chamber (see Fig. 1a) [21]. L1 focuses far-off-detuned laser light onto a waist of $1.2 \pm 0.1 \mu\text{m}$ ($1/e^2$ radius). This creates a dipole trap (depth: 1 mK) in which we load N atoms with a temperature of $120 \pm 15 \mu\text{K}$ [35]. We control the number of atoms N within 10%, and vary N between 10 and 180 [36]. The atomic cloud is cigar-shaped, with calculated transverse and longitudinal root-mean-square (rms) widths $(a_{\perp}, a_z) = (0.2, 1.2) \mu\text{m}$. The peak densities range from $n = 10^{13}$ to 2×10^{14} at/cm 3 . The uncertainties in the temperature, atom number and waist size lead to a systematic uncertainty on the peak density of a factor 2. The probe beam is focused down to a waist of $w = 1.20 \pm 0.05 \mu\text{m}$ also by L2 at the position of the cloud. It is linearly polarized and nearly resonant with the closed D2 transition of rubidium between the $(5S_{1/2}, F = 2)$ and $(5P_{3/2}, F = 3)$ levels at $\lambda = 2\pi c/\omega_0 = 780.2 \text{ nm}$ (linewidth $\Gamma = 2\pi \times 6 \text{ MHz}$) [37]. We operate the probe in the low intensity limit where the atoms respond linearly to the field: $I/I_{\text{sat}} \approx 0.04$ ($I_{\text{sat}} = 1.6 \text{ mW/cm}^2$). We collect the probe light transmitted through the cloud using L1 and couple it into a single-mode fiber connected to an avalanche photodiode (APD). The temporal signals are acquired by accumulating single photons using a counting card with a resolution of 150 ps. A polarization beam-splitter is placed before the single-mode fiber and aligned at 45° of the probe laser polarization so as to split the collected light between the

fibered APD and a CCD camera (not shown in Fig. 1a).

Our configuration is sensitive to the mode-matching $\mathcal{E}(\omega) = \int \{\mathbf{E}(\mathbf{r}, \omega) \cdot \mathbf{g}^*(\mathbf{r})\} dS$ between the total field $\mathbf{E} = \mathbf{E}_L + \mathbf{E}_{\text{sc}}$ and the mode \mathbf{g} of the single-mode-fibered detector (dS is a differential area element perpendicular to the optical axis) [22]. In the absence of atoms the fiber mode is matched to the incoming light, i.e. $\mathbf{g} \propto \mathbf{E}_L$. In our experiment, we measure $\langle |\mathcal{E}(\omega)|^2 \rangle$, where $\langle \cdot \rangle$ means an average over many realizations of the cloud. After averaging, the signal is the sum of two parts [23]: (i) $|\mathcal{E}_{\text{coh}}(\omega)|^2$ due to $\mathbf{E}_L + \langle \mathbf{E}_{\text{sc}} \rangle$, and (ii) $\langle |\mathcal{E}_{\text{incoh}}(\omega)|^2 \rangle$ due to the fluctuating field $\mathbf{E}_{\text{sc}} - \langle \mathbf{E}_{\text{sc}} \rangle$. In the direction of propagation of the laser $|\mathcal{E}_{\text{coh}}(\omega)|^2 \gg \langle |\mathcal{E}_{\text{incoh}}(\omega)|^2 \rangle$ (see below and in Fig. 1a) and we are therefore mainly sensitive to the coherent optical response, which we characterize by a transfer function $\mathcal{S}(\omega) = \langle \mathcal{E}(\omega) \rangle / \mathcal{E}_L(\omega)$ obtained by comparing the detected fields with and without atoms.

To measure $\mathcal{S}(\omega)$ in steady-state, we proceed in the following way: after preparing the atoms in the $(5S_{1/2}, F = 2)$ level, we switch off the dipole trap light during 500 ns and send a 300 ns probe pulse with a temporal top hat profile (rise time of 2 ns). We then recapture the cloud in the trap for 500 ns and repeat this release-probe-recapture 1000 times using the same atomic cloud [38]. This procedure is typically repeated with 200 different atomic clouds. A typical signal is shown in Fig. 1b. It reaches a steady-state after a transient time of ~ 26 ns, close to the lifetime $1/\Gamma$ of the excited state, during which the atomic medium gets polarized. We average the signal over a time interval of 120 ns (grey area) and normalize it with respect to the case without atoms to obtain the transmission in steady state for a given probe frequency. We checked that the scattered light has the same polarization as the probe light by rotating the polarizer P and observing a signal with a contrast of 95%, the same as in the absence of atoms. This feature is characteristic of the coherent scattered field, and therefore confirms experimentally that $|\mathcal{E}_{\text{coh}}(\omega)|^2 \gg \langle |\mathcal{E}_{\text{incoh}}(\omega)|^2 \rangle$. Finally, the sequence is repeated for various probe detunings $\Delta = \omega - \omega_0$ and atom numbers N . We obtain the spectra shown in Fig. 2a.

The derivation of a functional form for $\mathcal{S}(\omega)$ is very hard in our dense cloud regime. However in the case of a cloud with a size smaller than $1/k$ so that it behaves as a small dielectric sphere with a polarizability $\alpha_c(\omega)$ we get, following [22], $\mathcal{S}(\omega) \approx 1 + ik\alpha_c(\omega)/(\pi w^2)$, which we cast in the form:

$$\mathcal{S}(\omega) = 1 - \frac{A}{1 - 2i\frac{\omega - \omega_c}{\Gamma_c}}, \quad (1)$$

assuming that the polarizability is resonant around a frequency ω_c with a width Γ_c . We fit the spectra shown in Fig. 2a with the Lorentzian function $|\mathcal{S}(\omega)|^2$, using Eq. (1) and leaving A , $\Delta_c = \omega_c - \omega_0$ and Γ_c as free parameters. The fit agrees well with the data, confirming that the functional form of Eq. (1) is appropriate even for

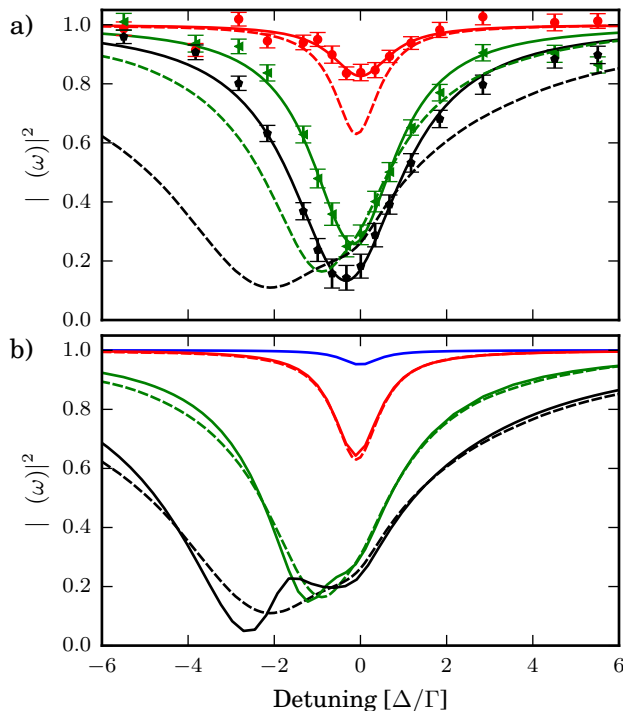


FIG. 2: (a) Measured transfer function of the cloud in steady-state versus probe detuning Δ for $N = (10, 83, 180)$ atoms (top to bottom); error bars: statistical (one standard deviation), shot noise limited. Solid lines: Lorentzian fit by $|S(\omega)|^2$. Dotted lines: results of the coupled dipole equations including the 12 levels of the $F_g = 2 - F_e = 3$ transition (see text). (b) Comparison between the predictions of the Lorentz model (solid line) and the microscopic, 12-level atom model (dotted line) for $N = (1, 10, 83, 180)$ (top to bottom).

our elongated sample. Figure 3 shows the results of the fits. For increasing atom numbers, we observe a saturation of the amplitude A , and therefore of the extinction, an increasing small red-shift and a broadening of the line. These behaviors can be understood qualitatively as a consequence of the dipole-dipole interactions between atoms, on the order of $\hbar\Gamma n/k^3$ (see below).

We now compare our results to various models of the optical response of the cloud. In Refs. [3, 24], Friedberg, Hartmann and Manassah used perturbation theory to derive the expressions for a collective decay rate and a collective shift for various geometries of an atomic ensemble of two-level atoms. There, the collective shift and rate are the real and imaginary parts of the average dipole-dipole interaction [25]. This theory predicts the “cooperative Lamb-shift” measured in a hot atomic vapor [5] and in a dilute, optically thick cold atomic sample [6]. For the case of an ellipsoidal cloud with Gaussian density distribution, the predictions (see formulae (5.2) and (5.3) of Ref. [24]) are plotted in Fig. 3b,c for our experimental parameters. Here, we included the rubidium internal structure by multiplying the prediction of Ref. [24] by the

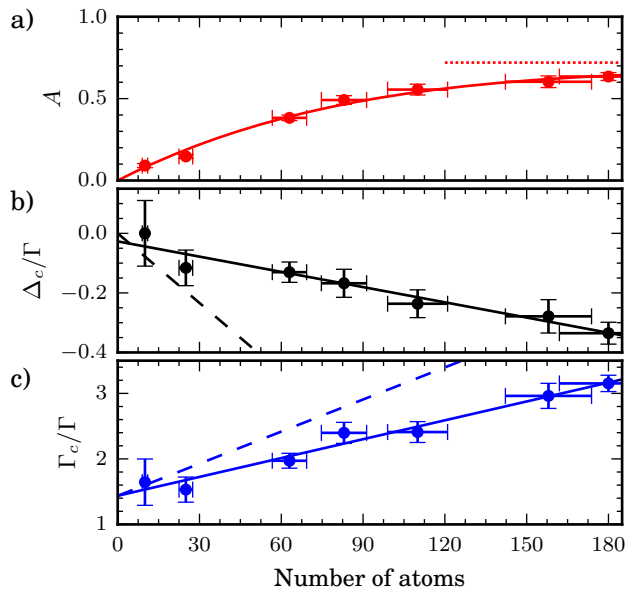


FIG. 3: Fit results of the data of Fig. 2 with the function $|S(\omega)|^2$. Error bars are from the fit. (a) Amplitude A . Solid green line: phenomenological fit to guide the eye, yielding a saturation (dotted line) at 0.7. (b) Shift of the center-frequency $\Delta_c = \omega_c - \omega_0$. Solid line: linear fit. (c) Full width at half maximum Γ_c . Solid line: linear fit. Dashed lines in (b) and (c): predictions by Friedberg, Hartmann and Manassah detailed in the text. The prediction for the width has been offset to match the data for $N = 0$.

ratio of multiplicities 7/15 of the $F_g = 2 - F_e = 3$ transition [26, 27], assuming equal populations in all hyperfine Zeeman ground states and a negligible magnetic field (as is the case in the experiment) [23]. The predictions differ significantly from the measured values, indicating that this perturbative approach does not apply for our dense, cold atomic systems.

To go beyond the FHM perturbative treatment, we now calculate the optical response as predicted by the Lorentz local field theory for our *dense* cigar-shaped cloud. For this purpose, we replace the cloud by a Gaussian continuous density distribution $n(\mathbf{r})$ (with rms widths a_\perp and a_z) and calculate the local susceptibility using the Lorentz-Lorenz formula $\chi(\mathbf{r}, \omega) = n(\mathbf{r})\alpha(\omega)/(1 - n(\mathbf{r})\alpha(\omega)/3)$ [1, 2]. Here $\alpha(\omega) = i(7/15)(6\pi/k^3)/[1 - i(2\Delta/\Gamma)]$ is the polarizability of a single atom, which includes the internal atomic structure of rubidium as described above, see [23]. We then define a local permittivity $\epsilon(\mathbf{r}) = 1 + \chi(\mathbf{r})$ and use a finite element program to calculate the electric field scattered in the far field by the cloud illuminated by the Gaussian laser beam. We finally compute the transfer function $S(\omega)$ taking for the Gaussian field the usual paraxial expression [23]. The results are shown in Fig. 2b. The mean-field response of the cloud predicted by the Lorentz-Lorenz formula deviates from the data as the number of atoms increases, featuring in particular a dou-

ble structure for the largest atom numbers [39], as well as a large asymmetry (also observed in the spectrum of transmitted light of an atomic slab described by the Lorentz-Lorenz formula [7]).

We finally calculate the coherent response of the cloud using a microscopic model where the atoms are considered as point-like dipoles \mathbf{d}_j randomly positioned according to the Gaussian spatial distribution, each being driven by the laser field and the fields scattered by all the other ones [11, 28]. This approach leads to a set of coupled dipole equations. As in Ref. [20], we include the internal structure of the atoms by randomly assigning them a given Zeeman state m_j of the ($5S_{1/2}, F=2$) manifold and we write $\mathbf{d}_j = \mathcal{D} \sum_{\sigma} \hat{\mathbf{e}}_{\sigma} C_{m_j}^{(\sigma)} \mathcal{P}_{j\sigma}$ ($\sigma = \pm 1, 0$ defines the polarization). The amplitude of the atomic dipole j associated to the optical transition $|g, m_j\rangle \rightarrow |e, m_j + \sigma\rangle$ is proportional to the reduced dipole matrix element \mathcal{D} , the atomic coherence $\mathcal{P}_{j\sigma}$, and the corresponding Clebsch-Gordan coefficient $C_{m_j}^{(\sigma)}$. We solve the steady state set of coupled equations for the coherences

$$(\Delta + i\Gamma/2) \mathcal{P}_{j\alpha} = \Omega_{j\alpha} + \sum_{l \neq j} \sum_{\beta} C_{m_l}^{(\beta)} C_{m_j}^{(\alpha)} V_{j\alpha}^{l\beta}(\mathbf{r}) \mathcal{P}_{l\beta},$$

where $V_{j\alpha}^{l\beta} = -V_{\text{dd}} [p_{\alpha\beta}(ikr - 1) + q_{\alpha\beta}(kr)^2] e^{ikr}$ with $V_{\text{dd}} = 3\hbar\Gamma/4(kr)^3$ is the dipole-dipole interaction, $p_{\alpha\beta}$ and $q_{\alpha\beta}$ are angular functions [20], and $\Omega_{j\alpha}$ the Rabi frequency. We calculate the field scattered by the cloud (yielding the radiation pattern shown in Fig. 1a). We then compute the interference of this field with the laser field, at the position of the lens L1, and the transfer function for this particular configuration of the atomic ensemble and average over many spatial configurations.

The results of the microscopic model are plotted in Fig. 2b for various detunings and atom numbers, together with the prediction of the Lorentz local field model. We observe that both models are in agreement for low values of N , and predict approximately Lorentzian lineshapes. For large atom numbers, however, they differ quantitatively, pointing towards the role of recurrent scattering, included in the microscopic model, to all orders, but not in the Lorentz model [9–11, 29, 30]. To the lowest order in density, for a cloud (density n) of identical atoms with polarizability α , the contribution of recurrent scattering to the susceptibility is proportional to the number of atom pairs $(n\alpha)^2$ inside the scattering volume α . It becomes important when $n\alpha \sim 1$. The onset of light-induced correlations and the effect of recurrent scattering as a function of the detuning and atom density was analyzed in more detail in [7, 10, 11, 31, 32]. In the presence of recurrent scattering and when $n/k^3 \ll 1$, the susceptibility takes the form:

$$\chi(\omega) = \frac{n\alpha(\omega)}{1 - n\alpha(\omega)(\frac{1}{3} + \beta(\omega))}, \quad (2)$$

where $\beta(\omega)$ is the contribution from recurrent scattering.

Using formula (22) of [10], we get $\beta(\omega) \propto B\alpha(\omega)k^3$, with B a volume integral challenging to calculate for our geometry. The lowest order contribution to β is independent of the density. If $B \sim 1$, the local field correction $n\alpha/3$ is thus on the same order as the recurrent scattering contribution close to resonance ($\alpha = 6\pi i/k^3$), while away from resonance ($\alpha k^3 \ll 1$) the influence of recurrent scattering is negligible. Remarkably, when inhomogeneous broadening is introduced (such as the Doppler effect in hot vapor cells [5]), the resonant frequencies of the dipoles j are spread over $\Delta\omega_D$ and β is replaced by the average over j , $\langle\alpha\rangle_j k^3$, and is therefore reduced by a factor $\Gamma/\Delta\omega_D$ [9]. This explains why for any medium where inhomogeneous broadening is dominant the Lorentz-Lorenz model is successful, as $\Gamma/\Delta\omega_D \ll 1$ and thus $\beta \ll 1$. On the contrary, in the absence of inhomogeneous broadening, the Lorentz-Lorenz formula is usually not valid at resonance. In [33], we use the microscopic approach to calculate the effective dielectric constant of our cloud, but in the regime $n/k^3 \geq 1$, and found that it does not follow the Lorentz-Lorenz formula, as expected.

Finally, we compare our measurements to the microscopic model (see Fig. 2a). We observe that the data are closer to this model than to the Lorentz model, as they do not show the double structure predicted by the Lorentz model for the largest atom numbers. This indicates that the Lorentz model is not valid in our configuration. However the measurements exhibit systematically less pronounced features for the shift, width and amplitude than predicted by the microscopic model. On the experimental side, we have ruled out possible biases, such as the probe beam alignment [23] and the possible cumulative heating of the cloud due to the pulsed illumination that could result in a modification of the cloud volume. On the theoretical side, the models ignore quantum fluctuations between hyperfine ground states and assume the low light intensity limit, which may in practice be difficult to fully realize in the experiments due to secondary radiation by closely-spaced atoms.

As a conclusion, we have measured the coherent scattering by a dense, cold atomic cloud. We have observed a failure of standard models, such as the FHM model or the mean-field Lorentz model. The remaining difference with the microscopic model shows that a quantitative understanding of the light-induced interactions even in a relatively simple situation is still a challenge.

We thank C.S. Adams for discussions. We acknowledge support from the E.U. (ERC Starting Grant ARENA and the HAIRS project), from the Triangle de la Physique (COLISCINA project), the labex PALM (ECONOMIC project) and the Region Ile-de-France (LISCOLEM project), the EPSRC, and the Leverhulme Trust. N.J. Schilder is supported by Triangle de la Physique. JJG is a senior member of the Institut Universitaire de France.

-
- [1] M. Born and E. Wolf, *Principle of Optics*, 7th ed. (Cambridge University Press, Cambridge, UK, 1999).
- [2] D.J. Jackson, *Classical Electrodynamics*, (John Wiley and Sons, New York, 1998).
- [3] R. Friedberg, S.R. Hartmann, and J.T. Manassah, Frequency shift and absorption by resonant systems of two-level atoms, *Phys. Rep.* **7**, 101 (1973).
- [4] R. Röhlsberger, K. Schlage, B. Sahoo, S. Couet, and R. Roeffer, Collective Lamb shift in single-photon superradiance, *Science* **328**, 1248 (2010).
- [5] J. Keaveney, A. Sargsyan, U. Krohn, I.G. Hughes, D. Sarkisyan, and C.S. Adams, Cooperative Lamb shift in an atomic vapor layer of nanometer thickness, *Phys. Rev. Lett.* **108**, 173601 (2012).
- [6] S.J. Roof, K.J. Kemp and M.D. Havey, I.M. Sokolov, Observation of single-photon superradiance and the cooperative Lamb shift in an extended sample of cold atoms, arXiv:1603.07268.
- [7] J. Javanainen and J. Ruostekoski, Light propagation beyond the mean-field theory of standard optics, *Optics Express*, **24**, 993 (2016).
- [8] S.E. Schnatterly and C. Tarrio, Local fields in solids: microscopic aspects for dielectrics, *Rev. Mod. Phys.* **64**, 619 (1992).
- [9] J. Javanainen, J. Ruostekoski, Y. Li and S.-M. Yoo, Shifts of a resonance line in a dense atomic sample, *Phys. Rev. Lett.* **112**, 113603 (2014).
- [10] O. Morice, Y. Castin and J. Dalibard, *Phys. Rev. A* **51**, 3896 (1995).
- [11] J. Ruostekoski and J. Javanainen, Quantum field theory of cooperative atom response: Low light intensity, *Phys. Rev. A* **55**, 513 (1997).
- [12] H. Bender *et al.*, Observation of cooperative Mie scattering from an ultracold atomic cloud, *Phys. Rev. A* **82**, 011404 (2010).
- [13] T. Bienaimé, S. Bux, E. Lucioni, Ph.W. Courteille, N. Piovella and R. Kaiser, *Phys. Rev. Lett.* **104**, 183602 (2010).
- [14] J. Chabé, M.-T. Rouabah, L. Bellando, T. Bienaimé, N. Piovella, R. Bachelard, and R. Kaiser, Coherent and incoherent multiple scattering, *Phys. Rev. A* **89**, 043833 (2014).
- [15] M. Chalony, R. Pierrat, D. Delande, and D. Wilkowski, Coherent flash of light emitted by a cold atomic cloud, *Phys. Rev. A* **84**, 011401 (2011).
- [16] C.C. Kwong *et al.*, Cooperative emission of a coherent superflash of light, *Phys. Rev. Lett.* **113**, 223601 (2014).
- [17] S. Roof, K. Kemp, M. Havey, I.M. Sokolov, and D.V. Kupriyanov, Microscopic lensing by a dense, cold atomic sample, *Opt. Lett.* **40**, 1137 (2015).
- [18] S.L. Bromley *et al.*, Collective atomic scattering and motional effects in a dense coherent medium, *Nat. Comm.* **7**, 11039 (2016).
- [19] M.O. Araújo, I. Kresic, R. Kaiser, W. Guérin, Superradiance in a large cloud of cold atoms in the linear-optics regime, arXiv:1603.07204.
- [20] J. Pellegrino *et al.*, Observation of suppression of light scattering induced by dipole-dipole interactions in a cold atom ensemble, *Phys. Rev. Lett.* **113**, 133602 (2014).
- [21] Y.R.P. Sortais *et al.*, Diffraction-limited optics for single-atom manipulation, *Phys. Rev. A* **75**, 013406 (2007).
- [22] S.A. Aljunid *et al.*, Phase shift of a weak coherent beam induced by a single atom, *Phys. Rev. Lett.* **103**, 153601 (2009).
- [23] See online Supplemental Material.
- [24] J.T. Manassah, Cooperative radiation from atoms in different geometries: decay rate and frequency shift, *Advances in Optics and Photonics* **4**, 108 (2012).
- [25] M.O. Scully, Collective Lamb Shift in Single Photon Dicke Superradiance, *Phys. Rev. Lett.* **102**, 143601 (2009).
- [26] J. Ruostekoski, Scattering of light and atoms in a Fermi-Dirac gas with Bardeen-Cooper-Schrieffer pairing, *Phys. Rev. A* **61**, 033605 (2000).
- [27] C.A. Müller, T. Jonckheere, Ch. Miniatura, and D. Delande, Weak localization of light by cold atoms: The impact of quantum internal structure, *Phys. Rev. A* **64**, 053804 (2001).
- [28] L. Chomaz, L. Corman, T. Yefsah, R. Desbuquois and J. Dalibard, Absorption imaging of a quasi-two-dimensional gas: a multiple scattering analysis, *New J. Phys.* **14**, 055001 (2012).
- [29] A. Lagendijk and B.A. van Tiggelen, Resonant multiple scattering of light, *Phys. Rep.* **270**, 143 (1996).
- [30] I.M. Sokolov, M.D. Kupriyanova, D.V. Kupriyanov, and M.D. Havey, Light scattering from a dense and ultracold atomic gas, *Phys. Rev. A* **79**, 053405 (2009).
- [31] R. Saunders and R.K. Bullough, Perturbation theory of super-radiance II. Cooperative and non-cooperative level shifts, *J. Phys. A* **6**, 1360 (1973).
- [32] J. Ruostekoski and J. Javanainen, Optical linewidth of a low density Fermi-Dirac gas, *Phys. Rev. Lett.* **82**, 4741 (1999).
- [33] N.J. Schilder, C. Sauvan, J.-P. Hugonin, S. Jennewein, Y.R.P. Sortais, A. Browaeys, and J.-J. Greffet, Polaritonic modes in a dense cloud of cold atoms, *submitted*, arXiv:1510.07993v2[physics.atom-ph].
- [34] Y.R.P. Sortais, A. Fuhrmanek, R. Bourgain, and A. Browaeys, Sub-Poissonian atom-number fluctuations using light-assisted collisions, *Phys. Rev. A* **85**, 035403 (2012).
- [35] The Doppler broadening ($k\Delta v = 0.06\Gamma$) is negligible with respect to the linewidth Γ .
- [36] The exact number of atoms inside the trap varies shot to shot as it is governed by a sub-Poisson distribution with a mean N and variance $3N/4$ [34].
- [37] The magnetic field is compensated to values lower than ~ 80 mG.
- [38] Our results vary by less than 5% when the same cloud is illuminated with a single shot probe. This observation rules out a possible cumulative modification of the cloud volume during the pulsed excitation.
- [39] The double structure appearing in the Lorentz model indicates that the resonance of the coherent response of the cloud is not only related to the resonance of the susceptibility, but also to a shape resonance.

Supplemental Material: Coherent scattering of near-resonant light by a Dense Microscopic Cold Atomic cloud

S. Jennewein,¹ M. Besbes,¹ N.J. Schilder,¹ S.D. Jenkins,² C. Sauvan,¹
J. Ruostekoski,² J.-J. Greffet,¹ Y.R.P. Sortais,¹ and A. Browaeys¹

¹*Laboratoire Charles Fabry, Institut d'Optique, CNRS, Univ Paris Sud,
2 Avenue Augustin Fresnel, 91127 Palaiseau cedex, France*

²*Mathematical Sciences, University of Southampton, Southampton SO17 1BJ, United Kingdom*

(Dated: April 29, 2016)

This Supplemental Material presents more details about the definition of the coherent transfer function $\mathcal{S}(\omega)$ and the expressions of the laser field used in the modeling. It also derives the mean-field expression of the susceptibility for a multi-level alkali atom that we use in the Lorentz-Lorenz formula to calculate the field scattered by the cloud. Finally, we discuss the influence on the line shape of a misalignment of the laser probe with respect to the atomic cloud.

I. COHERENT TRANSFER FUNCTION

The experimental configuration used in the experiment gives access to the overlap between the total field in the forward direction $\mathbf{E} = \mathbf{E}_L + \mathbf{E}_{sc}$ and the mode \mathbf{g} of the single-mode-fibered detector

$$\mathcal{E}(\omega) = \int \mathbf{E}(\mathbf{r}, \omega) \cdot \mathbf{g}^*(\mathbf{r}) dS \quad (1)$$

with dS a differential area element perpendicular to the optical axis. As the fiber mode is matched to the incoming light, $\mathbf{g} \propto \mathbf{E}_L$, and the total transfer function is

$$\mathcal{S}_{\text{tot}}(\omega) = \frac{\mathcal{E}(\omega)}{\mathcal{E}_L(\omega)} = \frac{\int \mathbf{E}(\mathbf{r}, \omega) \cdot \mathbf{E}_L^*(\mathbf{r}) dS}{\int |\mathbf{E}_L(\mathbf{r})|^2 dS}. \quad (2)$$

We then decompose the scattered field into the coherent and incoherent (fluctuating) components: $\mathbf{E}_{sc} = \langle \mathbf{E}_{sc} \rangle + \delta \mathbf{E}_{sc}$, where $\langle \cdot \rangle$ indicates an average over many spatial configurations of the cloud. In the experiment, we measure the configuration-averaged quantity

$$\begin{aligned} \langle |\mathcal{E}(\omega)|^2 \rangle &\propto \left| \int (\mathbf{E}_L + \langle \mathbf{E}_{sc} \rangle) \cdot \mathbf{E}_L^* dS \right|^2 \\ &+ \left\langle \left| \int \delta \mathbf{E}_{sc} \cdot \mathbf{E}_L^* dS \right|^2 \right\rangle, \end{aligned} \quad (3)$$

(taking into account $\langle \delta \mathbf{E}_{sc} \rangle = 0$), which we cast in the form $|\mathcal{E}_{\text{coh}}(\omega)|^2 + \langle |\mathcal{E}_{\text{incoh}}(\omega)|^2 \rangle$. As explained in the main text, $|\mathcal{E}_{\text{coh}}(\omega)|^2 \gg \langle |\mathcal{E}_{\text{incoh}}(\omega)|^2 \rangle$ in the direction of propagation of the laser, and therefore, we measure essentially the coherent part to the total transfer function. We thus define the coherent optical transfer function:

$$\mathcal{S}(\omega) = \frac{\langle \mathcal{E}(\omega) \rangle}{\mathcal{E}_L(\omega)} = 1 + \frac{\int \langle \mathbf{E}_{sc} \rangle \cdot \mathbf{E}_L^* dS}{\int |\mathbf{E}_L|^2 dS}. \quad (4)$$

In general, the transfer function defined above does not correspond to the transmission of the cloud defined as

$$T(\omega) = \frac{\langle \int |\mathbf{E}(\mathbf{r}, \omega)|^2 dS \rangle}{\int |\mathbf{E}_L(\mathbf{r})|^2 dS}. \quad (5)$$

If the solid angle of the collecting lens L1 is very small, $T(\omega)$ and $|\mathcal{S}_{\text{tot}}(\omega)|^2$ coincide. Otherwise, the relation between the transfer function and the transmission can be found by decomposing, once again, the total field as $\mathbf{E} = \mathbf{E}_L + \langle \mathbf{E}_{sc} \rangle + \delta \mathbf{E}_{sc}$. We then get

$$\begin{aligned} T(\omega) &= |\mathcal{S}(\omega)|^2 + \frac{\int \langle |\delta \mathbf{E}_{sc}|^2 \rangle dS}{\int |\mathbf{E}_L(\mathbf{r})|^2 dS} \\ &+ \frac{\int |\langle \mathbf{E}_{sc} \rangle|^2 dS}{\int |\mathbf{E}_L(\mathbf{r})|^2 dS} - \left| \frac{\int \langle \mathbf{E}_{sc} \rangle \cdot \mathbf{E}_L^* dS}{\int |\mathbf{E}_L(\mathbf{r})|^2 dS} \right|^2. \end{aligned} \quad (6)$$

Using the Cauchy-Schwartz inequality

$$\left| \int \langle \mathbf{E}_{sc} \rangle \cdot \mathbf{E}_L^* dS \right|^2 \leq \int |\langle \mathbf{E}_{sc} \rangle|^2 dS \int |\mathbf{E}_L(\mathbf{r})|^2 dS$$

yields $|\mathcal{S}(\omega)|^2 \leq T(\omega)$.

II. DESCRIPTION OF THE PROBE LASER FIELD

In the theoretical models (Lorentz local-field and microscopic), we use the following paraxial approximation for the amplitude of the x component of the electric probe laser field (with a waist w , see Fig. 1a in main text):

$$E_{L,x}(x, y, z) = \frac{E_0}{1 + i \frac{z}{z_R}} \exp \left[ik \frac{x^2 + y^2}{2q(z)} \right] \exp[ikz], \quad (7)$$

with $\frac{1}{q(z)} = \frac{1}{R(z)} + \frac{2i}{kw^2(z)}$, $z_R = kw^2/2$ the Rayleigh length, $w(z) = w\sqrt{1 + z^2/z_R^2}$ and $R(z) = z + z_R^2/z$.

As is well-known, this paraxial expression is not an exact solution of Maxwell's equation. We have therefore checked, for the calculation of the transfer function based on the Lorentz-Lorenz formula, that the field scattered by the cloud using the paraxial approximation is numerically very close to the one obtained by using the plane wave decomposition of the incident beam (which corresponds to an exact solution of Maxwell's equations).

III. DERIVATION OF THE MEAN-FIELD SUSCEPTIBILITY FOR A MULTI-LEVEL ATOM

In this section we derive the mean-field electric susceptibility for a multi-level atom, when the recurrent scattering contributions are ignored. This is then used in the main section of the paper to calculate the mean-field response and the “cooperative Lamb shift” for a ^{87}Rb $F = 2$ ground-state manifold that differ from the ones obtained for an isotropic $F = 0 \rightarrow F' = 1$ transition.

We use the general formalism of Ref. [1] and derive the multi-level electric susceptibility as in Ref. [2]. We consider an atom with ground states $|g, \nu\rangle$ and excited states $|e, \eta\rangle$. Here ν and η represent the Zeeman sub-levels of the ground and excited states, respectively, separated by a transition at a frequency ω_0 .

The positive frequency component of the electric field amplitude is the sum of the incident coherent field $\mathbf{D}_F^+(\mathbf{r})$ and the scattered field from the atomic polarization $\hat{\mathbf{P}}^+(\mathbf{r})$,

$$\epsilon_0 \hat{\mathbf{E}}^+(\mathbf{r}) = \mathbf{D}_F^+(\mathbf{r}) + \int d^3r' \mathbf{G}(\mathbf{r} - \mathbf{r}') \hat{\mathbf{P}}^+(\mathbf{r}'). \quad (8)$$

The monochromatic dipole radiation kernel $\mathbf{G}(\mathbf{r})$ [3] gives the radiated field at \mathbf{r} from a dipole with the amplitude $\hat{\mathbf{d}}$ residing at the origin:

$$\mathbf{G}(\mathbf{r}) \hat{\mathbf{d}} = \frac{k^3}{4\pi} \left\{ (\hat{\mathbf{n}} \times \hat{\mathbf{d}}) \times \hat{\mathbf{n}} \frac{e^{ikr}}{kr} + [3\hat{\mathbf{n}}(\hat{\mathbf{n}} \cdot \hat{\mathbf{d}}) - \hat{\mathbf{d}}] \left[\frac{1}{(kr)^3} - \frac{i}{(kr)^2} \right] e^{ikr} \right\} - \frac{\hat{\mathbf{d}} \delta(\mathbf{r})}{3}, \quad (9)$$

where $k = \omega/c$, ω denotes the laser light frequency, and $\hat{\mathbf{n}} = \mathbf{r}/r$.

Using the second quantized atomic field operators $\hat{\psi}_{g\nu}(\mathbf{r})$ and $\hat{\psi}_{e\eta}(\mathbf{r})$, the positive frequency component of the atomic polarization density can be written in terms of contributions from different sub-level transitions as

$$\hat{\mathbf{P}}^+(\mathbf{r}) = \sum_{\nu, \eta} \hat{\mathbf{P}}_{\nu\eta}^+(\mathbf{r}), \quad (10)$$

$$\hat{\mathbf{P}}_{\nu\eta}^+(\mathbf{r}) \equiv \mathbf{d}_{g\nu e\eta} \hat{\psi}_{g\nu}^\dagger(\mathbf{r}) \hat{\psi}_{e\eta}(\mathbf{r}), \quad (11)$$

where $\mathbf{d}_{g\nu e\eta}$ represents the dipole matrix element for the transition $|e, \eta\rangle \rightarrow |g, \nu\rangle$

$$\mathbf{d}_{g\nu e\eta} \equiv \mathcal{D} \sum_{\sigma} \hat{\mathbf{e}}_{\sigma} \langle e\eta; 1g | 1\sigma; g\nu \rangle \equiv \mathcal{D} \sum_{\sigma} \hat{\mathbf{e}}_{\sigma} \mathcal{C}_{\nu, \eta}^{(\sigma)}. \quad (12)$$

Here the sum is over the unit circular polarization vectors $\sigma = \pm 1, 0$, and $\mathcal{C}_{\nu, \eta}^{(\sigma)}$ denote the Clebsch-Gordan coefficients of the corresponding optical transitions. The reduced dipole matrix element \mathcal{D} is related to the linewidth of the transition Γ by

$$\Gamma = \frac{\mathcal{D}^2 \omega_0^3}{3\pi \hbar \epsilon_0 c^3}, \quad (13)$$

and $\mathbf{d}_{e\eta g\nu} = \mathbf{d}_{g\nu e\eta}^*$. The light fields with the polarizations $\hat{\mathbf{e}}_{\pm}$ and $\hat{\mathbf{e}}_0$ drive the transitions $|g, \nu\rangle \rightarrow |e, \nu \pm 1\rangle$ and $|g, \nu\rangle \rightarrow |e, \nu\rangle$, respectively, in such a way that only the terms $\sigma = \eta - \nu$ in Eq. (12) are nonvanishing.

As described in Refs. [1, 2], in the limit of low light intensity we obtain the equation of motion for the expectation value of the polarization component $\mathbf{P}_{\nu\eta}^+(\mathbf{r}) = \langle \hat{\mathbf{P}}_{\nu\eta}^+(\mathbf{r}) \rangle$,

$$\begin{aligned} \frac{d}{dt} \mathbf{P}_{\nu\eta}^+(\mathbf{r}) = & (i\bar{\Delta}_{g\nu e\eta} - \frac{\Gamma}{2}) \mathbf{P}_{\nu\eta}^+(\mathbf{r}) + i\xi \rho_{\nu}(\mathbf{r}) \mathbf{P}_{\eta\nu}^{\nu\eta} \mathbf{D}_F^+(\mathbf{r}) \\ & + i\xi \int d^3r' \mathbf{P}_{\eta\tau}^{\nu\eta} \mathbf{G}(\mathbf{r} - \mathbf{r}') \langle \hat{\psi}_{g\nu}^\dagger(\mathbf{r}) \hat{\mathbf{P}}^+(\mathbf{r}') \hat{\psi}_{g\tau}(\mathbf{r}') \rangle, \end{aligned} \quad (14)$$

where we assumed that there are no ground-state coherences between the different hyperfine states, so that $\langle \hat{\psi}_{g\nu}^\dagger \hat{\psi}_{g\tau} \rangle = \delta_{\nu, \tau} \rho_{\nu}$, with ρ_{ν} the atom density of the ground state $|g, \nu\rangle$.

We have defined $\xi = \mathcal{D}^2 / (\hbar \epsilon_0)$ and $\Delta_{ab\eta} = \Delta_{b\eta} - \Delta_{a\nu}$ ($a, b = g, e$). In the presence of a magnetic field B , the atom-light detuning is $\Delta_{e\eta} = \omega - (\omega_0 + \mu_B B g_l^{(e)} \eta / \hbar)$ and $\Delta_{g\nu} = -\mu_B B g_l^{(g)} \nu / \hbar$, with ω denoting the frequency of the incident light, and $g_l^{(g)}$ and $g_l^{(e)}$ the Landé factors of the ground and excited states, respectively. In Eq. (14) we also introduced the tensor

$$\mathbf{P}_{\mu\tau}^{\nu\eta} \equiv \frac{\mathbf{d}_{g\nu e\eta} \mathbf{d}_{e\mu g\tau}}{\mathcal{D}^2} = \sum_{\sigma, \varsigma} \hat{\mathbf{e}}_{\sigma} \hat{\mathbf{e}}_{\varsigma}^* \mathcal{C}_{\nu, \eta}^{(\sigma)} \mathcal{C}_{\tau, \mu}^{(\varsigma)}. \quad (15)$$

The pair correlation function $\langle \hat{\psi}_{g\nu}^\dagger(\mathbf{r}) \hat{\mathbf{P}}^+(\mathbf{r}') \hat{\psi}_{g\tau}(\mathbf{r}') \rangle$ describes light-induced correlations between the atoms at \mathbf{r} and \mathbf{r}' [1]. These correlations are non-trivial in the presence of recurrent scattering processes. In the mean-field theory we neglect recurrent scattering by the decorrelation approximation $\langle \hat{\psi}_{g\nu}^\dagger(\mathbf{r}) \hat{\mathbf{P}}^+(\mathbf{r}') \hat{\psi}_{g\tau}(\mathbf{r}') \rangle \simeq \rho_{\nu}(\mathbf{r}) \mathbf{P}^+(\mathbf{r}')$ in Eq. (14).

We are interested in the steady-state solution of the resulting approximation to Eq. (14). In the interaction potential between the two atoms in Eq. (14), we can now remove the contact term $\mathbf{G}(\mathbf{r}) \rightarrow \mathbf{G}(\mathbf{r}) + \delta(\mathbf{r})/3$, and then eliminate the scattered field between Eqs. (14) and (8) (this procedure can be derived rigorously [4]). We obtain

$$\mathbf{P}_{\nu\eta} = \alpha_{\nu\eta} \rho_{\nu} \mathbf{P}_{\eta\nu}^{\nu\eta} (\epsilon_0 \mathbf{E} + \mathbf{P}/3), \quad (16)$$

where the polarizability is given by

$$\alpha_{\nu\eta} = -\frac{\mathcal{D}^2}{\hbar \epsilon_0} \frac{1}{\Delta_{g\nu e\eta} + i\frac{\Gamma}{2}}. \quad (17)$$

Equation (16) now leads to a coupled set of linear equations between the different polarization components [2] that can be solved

$$\mathbf{P}_{\nu\eta} = \frac{\alpha_{\nu\eta} \rho_{\nu} [\mathcal{C}_{\nu, \eta}^{(\sigma')}]^2}{1 - \sum_{\tau, \varsigma} \alpha_{\tau\varsigma} \rho_{\tau} [\mathcal{C}_{\tau, \varsigma}^{(\sigma')}]^2 / 3} \epsilon_0 (\hat{\mathbf{e}}_{\sigma'}^* \cdot \mathbf{E}) \hat{\mathbf{e}}_{\sigma'}, \quad (18)$$

where $\sigma' = \eta - \nu$. The sum in the denominator therefore includes the components for which $\mathcal{C}_{\tau,\zeta}^{(\sigma')} \neq 0$, i.e., the components for which $\mathbf{P}_{\tau,\zeta}$ is parallel to $\mathbf{P}_{\nu,\eta}$.

We can then separate the different vector components of the total polarization $\mathbf{P} = \sum_{\nu,\eta} \mathbf{P}_{\nu,\eta}$ by considering each value of the spherical polarization component σ' separately

$$\hat{\mathbf{e}}_{\sigma'}^* \cdot \mathbf{P} = \frac{\sum_{\nu,\eta} \alpha_{\nu\eta} \rho_{\nu} [\mathcal{C}_{\nu,\eta}^{(\sigma')}]^2}{1 - \sum_{\tau,\zeta} \alpha_{\tau\zeta} \rho_{\tau} [\mathcal{C}_{\tau,\zeta}^{(\sigma')}]^2 / 3} \epsilon_0 (\hat{\mathbf{e}}_{\sigma'}^* \cdot \mathbf{E}). \quad (19)$$

This now gives the electric susceptibility for $\sigma' = \pm 1, 0$.

To describe the experiment (for which the magnetic field is $B \approx 0$ G), we consider a linearly polarized laser beam driving π transitions ($\sigma = 0$). We also assume all the Zeeman states of the ground level $F = 2$ equally populated, implying $\rho_{\nu} = \rho_{\text{total}}/5$. In this way, the only effect of the internal structure of the atom is to multiply the polarizability given by Eq. (17) (with $\Delta_{g\nu\eta} = \Delta = \omega - \omega_0$) by $\sum_{\nu} [\mathcal{C}_{\nu,\nu}^{(0)}]^2 / 5 = 7/15$, as written in the main text.

IV. INFLUENCE OF A MISALIGNMENT OF THE PROBE WITH RESPECT TO THE CLOUD

In this last section, we analyze the influence of a misalignment of the probe with respect to the atomic cloud. The dimensions of the cloud are $(a_{\perp}, a_z) = (0.2, 1.2) \mu\text{m}$, to be compared to the probe beam waist $w = 1.20 \pm 0.05 \mu\text{m}$. These very small numbers indicate that the perfect alignment of the probe with respect to the cloud is challenging. As demonstrated in [5], a longitudinal displacement of the probe focal point with respect to the center of the cloud leads to asymmetric atomic line shapes in transmission. Reference [5] interprets this asymmetry as a lensing effect induced by the cloud.

We have modeled the effect of a misalignment of the probe using the coupled dipole equations. We calculate the transfer function as described in the main text for different transverse and longitudinal positions of the cloud with respect to the probe beam. Figure 1a presents the results for a longitudinal displacement of the cloud along the direction of propagation of the probe beam for $N = 20$ atoms. We observe a strong asymmetry of the line shape when the cloud is displaced by $\pm z_R$ with respect to the position of the beam waist. This asymmetry can be understood as an effect of the Gouy phase of the probe laser (see below).

Finally, we displace transversally the atomic cloud in the focal plane of the laser beam, perpendicular to the optical axis. The results are shown in Fig. 1b. The main effect of the displacement is to reduce the amplitude of the line, without inducing any frequency shift or any change in the linewidth. We have tested that this conclusion remains valid for all atom numbers investigated in this

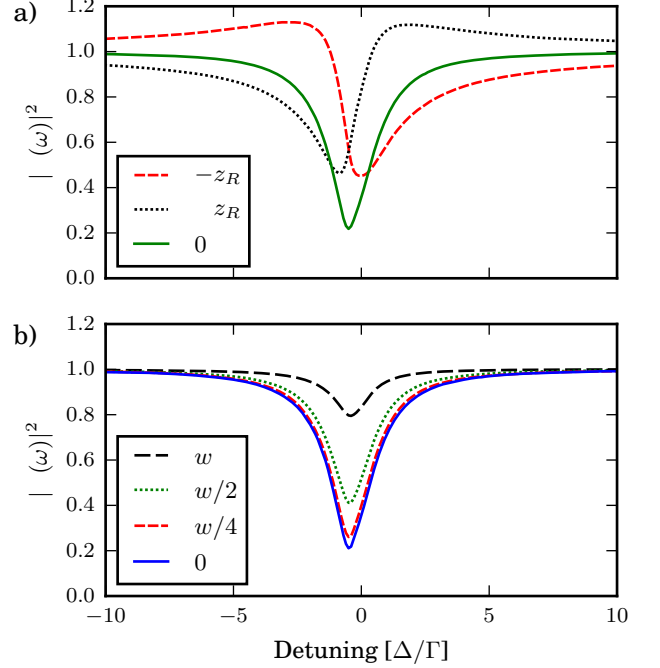


FIG. 1: (a) Influence of a longitudinal displacement of the position of the waist of the probe beam with respect to the center of the atomic cloud. The focus of the beam is displaced by $z_0 = \pm z_R$, with respect to the position of the center of the cloud ($z_0 = 0$). (b) Influence of a transverse misalignment of the probe beam with respect to the center of the atomic cloud. We considered 3 transverse displacements with respect to the center of the cloud (0): $w/4$, $w/2$ and w , where $w = 1.2 \mu\text{m}$ is the probe beam waist. Both (a) and (b) correspond to $N = 20$.

work. In particular, the transverse displacement does not induce any extra asymmetry in the line shape with respect to the case of an unshifted position of the cloud.

Both effects can be understood using the following simplified model. Let us consider the case of a dielectric cloud with a size smaller than $1/k$ (k is the wave-vector of the light) with a polarizability $\alpha(\omega)$ (with a width Γ_c and a central frequency ω_c), located at a position (x_0, y_0, z_0) around the focal point of the probe beam at position $(0, 0, 0)$. At a distance $z \gg |x_0|, |y_0|, |z_0|$ in the far-field, the component of the electric field along the x -axis scattered by the cloud in the direction of the propagation of the probe (z axis) is [3]:

$$E_{sc,x}(z) \approx \frac{k^2}{4\pi} \alpha(\omega) |E_L(x_0, y_0, z_0)| e^{i[\psi(z_0) + kz_0]} \times \frac{e^{ik\sqrt{(z-z_0)^2 + x_0^2 + y_0^2}}}{z}, \quad (20)$$

with $\psi(z_0)$ the Gouy phase given by $\psi(z_0) = -\arctan[z_0/z_R]$. Using the far-field expression of the laser electric field (7), we get the total field in the di-

rection of propagation of the probe:

$$E_{\text{tot},x} = -i \frac{z_R}{z} |E_L(0)| e^{ikz} \times \left(1 + i \frac{k^2 \alpha(\omega)}{4\pi z_R} \frac{|E_L(x_0, y_0, z_0)|}{|E_L(0)|} e^{i\psi(z_0)} \right). \quad (21)$$

Along the axis, the transfer function is:

$$\frac{E_{\text{tot},x}}{E_{L,x}} = 1 + i \frac{k^2 \alpha(\omega)}{4\pi z_R} \frac{|E_L(x_0, y_0, z_0)|}{|E_L(0)|} e^{i\psi(z_0)}, \quad (22)$$

which can be cast in the form of an on-axis transfer function:

$$\mathcal{S}_{\text{axis}}(\omega) = 1 - \frac{A}{1 - 2i \frac{\omega - \omega_c}{\Gamma_c}} e^{i\psi(z_0)}, \quad (23)$$

with A a real number. This expression shows that for a cloud located at $(x_0, y_0, 0)$ (transverse displacement), the amplitude of the extinction is attenuated by the ratio $|E_L(x_0, y_0, z_0)|/|E_L(0)|$, as observed in Fig. 1(b). When

the cloud is centered in $(0, 0, z_0)$ (with z_0 small but not negligible with respect to z_R), the phase factor $e^{i\psi(z_0)}$ involving the Gouy phase leads to an asymmetric function of ω : this explains the asymmetry observed in Fig. 1a. From the very slight asymmetry observed on the data (see Fig. 1a of the main text), we infer the phase $\psi(z_0)$ by fitting the data by the expression $|\mathcal{S}_{\text{axis}}(\omega)|^2$ (Eq. 23). We find $\psi(z_0) \approx 0.3$ rad and extract a longitudinal displacement of the cloud $z_0 \approx 1.8 \mu\text{m}$. Importantly, we find that this phase is independent of the atom number, as it should if it is a geometric phase. A lensing effect would lead to an asymmetry that would vary with the number of atoms.

We conclude from this study that a misalignment of the probe cannot introduce any narrowing of the line or any extra shift, nor wash out any double structure. The misalignment thus cannot explain the discrepancy between the theoretical models and the data, which systematically feature a smaller shift and linewidth and no significant asymmetry.

-
- [1] J. Ruostekoski and J. Javanainen, Quantum field theory of cooperative atom response: Low light intensity, *Phys. Rev. A* **55**, 513 (1997).
 - [2] J. Ruostekoski, Scattering of light and atoms in a Fermi-Dirac gas with Bardeen-Cooper-Schrieffer pairing, *Phys. Rev. A* **55**, 513 (2000).
 - [3] D.J. Jackson, *Classical Electrodynamics*, (John Wiley and Sons, New York, 1998).
 - [4] J. Ruostekoski and J. Javanainen, Lorentz-Lorenz shift in a Bose-Einstein condensate, *Phys. Rev. A* **56**, 2056 (1997).
 - [5] S. Roof, K. Kemp, M. Havey, I.M. Sokolov, and D.V. Kupriyanov, Microscopic lensing by a dense, cold atomic sample, *Opt. Lett.* **40**, 1137 (2015).